Science Requirements for Passive Microwave Sensors on Earth Science Geostationary Platforms

A.J. Gasiewski and D.H. Staelin
Research Laboratory of Electronics
Massachusetts Institute of Technology
Cambridge, Massachusetts

1 Meteorological Considerations

The science requirements for a passive geosynchronous microwave sounder are dictated by 1) the spectrum of oxygen, water vapor, and liquid and frozen hydrometeors, 2) the spatial and temporal scales for variation of atmospheric temperature, water vapor, and precipitation, 3) the area of the region to be mapped, 4) receiver sensitivity, 5) the geosynchronous observation geometry. Specifications for a spaced-based antenna and receiver are determined from these requirements.

Vertical sounding of atmospheric temperature can be performed using channels within the 5-mm O_2 absorption band (near 60-GHz) and the 118.75-GHz O_2 absorption line (Fig. 1 and Table 1) [1,2], although the 118-GHz line offers higher spatial resolution for diffraction-limited apertures of fixed size. Water vapor sounding can be performed using channels near the 183-GHz H_2O absorption line, although the weaker 22-GHz H_2O line is also useful for integrated water vapor retrieval [3,4]. Window channels at frequencies adjacent to the O_2 and H_2O lines facilitate the estimation of surface emissivity, which impacts both passive temperature and water vapor retrievals. Since precipitation exhibits only broad spectral features, sounding requires channels

Table 1: List of channels for passive sounding of tropospheric temperature, clouds and water vapor, and precipitation. The primary (P) channels are required for retrieval of the particular meteorological parameter, while the secondary (S) channels provide useful information to support retrievals.

Frequency (GHz) and # of channels	Meteorological Parameter			Comments
	Temperature	Water Vapor	Precipitation	
6 (1)			P	Window
10 (1)			P	Window
18 (1)			P	Window
22 (1)		S		H_2O line
31-37 (1)	S		P	Window
50-60 (5)	P		P	O_2 Complex
90-110 (1)	S	S	P	Window
118 (8-11)	P		P	O_2 line
166 (1)	S	P	P	Window
183 (3-4)		P		H_2O line
220-230 (1)		S	P	Window

distributed over a decade in frequency [5,6]. These include window channels near 6, 10, 18, 31-37, and 90-110 GHz, which are particularly useful over ocean; 6 and 10 GHz are the most accurate over heavy precipitation (> 15 mm/hr) and 31-110 GHz are sensitive to weaker precipitation ($\leq$ 15 mm/hr) and ice scattering by glaciated cell tops. Oxygen channels at 50-60 and 118 GHz are particularly useful over land because of the altitude-probing property of the weighting functions; these can be used to retrieve cell top altitude. Additional channels near 160 and 220 GHz provide higher precipitation sensitivity over land and diffraction-limited spatial resolution than any lower frequency precipitation channels.

The primary advantage of geosynchronous observations is the ability to monitor rapidly evolving meteorological processes, such as hurricanes, strong convection, water vapor transport, and temperature anomalies. Precipitation should ideally be observed at intervals as short as 10 minutes, although complete disk coverage at this rate would not be necessary. Slightly less stringent temporal requirements must be met for observation of water vapor. In the case of atmospheric temperature, which does not evolve as quickly as water vapor or precipitation, observation intervals as short as 30 minutes are desirable, but observations separated by up to 2 hours are useful. When used in conjunction with full-disk infrared (IR) sounders, a passive microwave sounder covering 20% of the Earth's disk with a scan time of 1 hour would be adequate for observing regions obscured by IR-blocking clouds, with the proviso that the scanned region can be arbitrarily selected. Passive microwave coverage of the full disk every 10 minutes would be ideal.

The sizes of convective precipitation cells have been observed to vary from $\sim$2 km to over 200 km. Over deep convection, brightness perturbations have been observed to be as large as -200 K near 90 GHz, 183 GHz, and the transparent channels near 118 GHz [7,8,9]. Such microwave brightness temperature structure is comparable with atmospheric temperature structure associated with severe storms. Indeed, horizontal atmospheric temperature gradients as high as 1 °C/km have been measured in the eyes of hurricanes [10]. Morphological information from brightness imagery is useful for distinguishing thermal and precipitating events, however, without sufficient spatial resolution, cold, spatially unresolved precipitation cells and atmospheric temperature or water vapor anomolies can be indistinguishable by their brightness temperature signatures. Hence, 3-dB footprints smaller than 2 km at 220 GHz are ultimately desirable for both unambiguous retrievals of atmospheric temperature and water vapor, and detection of precipitation, although 3-dB footprints up to 20 km in diameter at this frequency would still be useful. Similar spatial resolution is ultimately desirable at frequencies as low as 6 GHz, but will be much more difficult to obtain.

Although polarization information has been shown to be useful in the retrieval

of precipitation at slant angles over water [11], the inclusion of vertical and horizontal polarization sensitivity is not deemed to be of primary importance. This is especially true for microwave frequencies above 100 GHz, where passive observations of precipitation are essentially unpolarized.

In summary, the requirements for the geosynchronous remote sensing of atmospheric temperature, water vapor, clouds, and precipitation are shown in Tables 2, 3, and 4. These requirements are categorized as "adequate" and "ideal"; the adequate microwave requirements are necessary for any significant improvement in hydrologic cycle observability, and assume IR coverage of clear-air and broken-cloud regions. The ideal requirements indicate a transition to a region of diminishing scientific returns on the hardware investment.

Table 2: Requirements for passive microwave temperature sounding from geosynchronous orbit.

	Adequate	Ideal
Frequency (GHz)	110-120	50-120
Coverage	20% of disk/hr	full disk
Spatial Resolution		
at 120 GHz	50 km	20 km
Temporal Resolution	30-120 min	30 min
Radiometric Accuracy	$\leq$ 1.5 K	$\leq$ 0.5 K
Radiometric Sensitivity	$\leq$ 0.5 K	$\leq$ 0.2 K

Table 3: Requirements for passive microwave cloud and water vapor sounding from geosynchronous orbit.

	Adequate	Ideal
Frequency (GHz)	110-183	22-183
Coverage	20% of disk/hr	full disk
Spatial Resolution		
at 183 GHz	30-50 km	10 km
Temporal Resolution	30-120 min	10-30 min
Radiometric Accuracy	$\leq$ 1.5 K	$\leq$ 0.5 K
Radiometric Sensitivity	$\leq$ 0.6 K	$\leq$ 0.3 K

Table 4: Requirements for passive microwave precipitation sounding from geosynchronous orbit.

	Adequate	Ideal
Frequency (GHz)	110-220	6-220
Coverage	10% of disk/hr	full disk
Spatial Resolution	20 km @ 220 GHz	6 km @ 6 GHz
Temporal Resolution	30-60 min	10-30 min
Radiometric Accuracy	≤ 3 K	≤ 1.5 K
Radiometric Sensitivity	≤ 0.5 K	≤ 0.3 K

2 General Antenna and Receiver Considerations

The radiometric sensitivity is most critical for the retrieval of atmospheric temperature and water vapor, and should be no worse than 0.5 K for the O_2 channels, and comparable for the H_2O channels. Small biases in the sensor calibration can be accounted for by in-flight comparison against forward transfer calculations based on radiosonde measurements. However, the absolute accuracy of the instrument should be kept to within 2 to 3 times the radiometric sensitivity. The sensitivity and accuracy requirements are slightly less rigid for the precipitation channels. Precise in-flight sensor calibration using two known brightness temperatures is necessary to achieve this accuracy. Careful attention must be given to calibration errors due to internal reflections and receiver nonlinearities.

In order to meet the sensor sensitivity requirements for all spots, constraints on the antenna efficiency and sidelobe levels are necessary. The constraints can be discussed by defining five angular regions, as in Fig. 2 :

1) **Main lobe.** The main lobe region includes all angles within the first antenna pattern null, and subtends approximately $3.26\lambda/D$ radians for a filled aperture with a linear field illumination taper, where D is the aperture diameter and λ is the wavelength. In this case, the peak main lobe gain G_M is approximately $0.75\,(\pi D/\lambda)^2$, or $G_M = 102.1 - 20\log R$ dBI (decibels relative to isotropic), where R is the desired 3-dB equatorial footprint size (in km). An aperture efficiency of 75% has been assumed [12]. Thus, for spatial resolutions R of 2 to 20 km, the required main lobe gains are 96 to 76 dBI, respectively.

The main lobe efficiency is the fraction of the total captured power from within the main lobe region. This should exceed 95%, (and more ideally 97%). The corresponding average sidelobe level over all angles outside the main lobe becomes -13 dBI (ideally -15 dBI), although more stringent constraints on the peak sidelobe levels must be met for specific angular regions.

2) **Near-sidelobes.** The near-sidelobe region is defined to be the angular region within approximately 10 to 15 beamwidths of the the main lobe, but not including the main lobe. In this region, sidelobe levels will necessarily be the largest, comprising approximately 3% (ideally 2%) of the total stray radiation. Some enhancement of the raw image can be achieved via deconvolution of the near-sidelobe antenna pattern.

3) **Limb sidelobes.** The limb sidelobe region is the angular region (outside of the near sidelobe region) containing all angles which cross the Earth's limb during a full disk scan. The sidelobes in the limb region will alternately view cold space (2.7 K) and the Earth's disk ($\sim$ 250 K), depending upon the particular spot being

observed. Thus, the limb-sidelobe region subtends an angle of 17.4°. By requiring the maximum antenna temperature fluctuation due to the sweep of limb sidelobes to be less than 0.05 K, a constraint is placed on the average limb sidelobe level, which can be met by requiring that the peak limb sidelobe level G_L remain below -13.6 dBI, or, relative to the main lobe gain, $G_L \leq -115.7 + 20 \log R$ dB. Thus, for 2 to 20 km spatial resolution, all limb sidelobes should remain at least 110 to 90 dB below the main lobe gain, respectively. Within these constraints, the maximum stray radiation from the limb region will remain less than 0.03%. Relaxing the maximum limb-sweep antenna temperature fluctuation to 0.2 K reduces the limb sidelobe constraint by only 6 dB.

4) **Ecliptic sidelobes.** The ecliptic region is defined to contain all angles which directly view the sun or moon. Thus, the ecliptic region is an angular strip bounded at the elevation angles $\epsilon = \pm 37.9°$, and subtending the ecliptic plane. The sun can be modelled as a blackbody of temperature between 6,000 K (at 220 GHz) and 10,000 K (at 6 GHz), and subtends an angle of 0.53° . (The moon subtends nearly the same angle, but exhibits a brightness temperature less than 400 K, and hence can be negelected.) Within the ecliptic region, all radiometric fluctuations due to the passage of the sun through the antenna sidelobes should remain less than 0.05 K. This is satisfied by requiring that all ecliptic sidelobes levels remain below 0 dBI, or at least $102.1 - 20 \log R$ dB below the main lobe gain. This is a less stringent requirement than for the limb sidelobe levels, but is particularly important for antennas exhibiting grating lobes, for example, thinned arrays.

5) **Ortho-ecliptic sidelobes.** The ortho-ecliptic region is the complement of the ecliptic region, and contains all angles which never directly view the sun, moon, or Earth. In this region, the peak sidelobe level can rise to values above isotropic (0 dBI), provided that the main lobe efficiency requirement is met. Thus, the maximum stray radiation from the ecliptic and ortho-ecliptic regions should remain below 2% (ideally 1%), requiring the average sidelobe level over these two regions to remain below -17 dBI (ideally -20dBI).

3 Implementation using a Filled-Aperture Sensor

For filled-aperture sensors with linear field illumination taper, the 3-dB beamwidth $\theta_{3dB} = 1.3\lambda/D$, and the required diameter for a given equatorial resolution R is $D(\text{m}) \approx 13900/\left(f(\text{GHz})\ R(\text{km})\right)$ (see Table 5). The 3-dB footprint at 60° latitude will cover approximately 3.2 times the area as at the equator.

The spatial and temporal observation requirements place constraints on the available integration time per spot τ, as suggested in Table 6 for a single-spot, filled-

aperture sensor. In this arrangement, a single feed assembly is used by all channels, although the feed assembly might consist of more than one feed horn to accomodate channels over a wide frequency range. The brightness sensitivity of a radiometer operated in the total power mode is given by:

$$\Delta T_{RMS} = \frac{T_R + T_A}{\sqrt{B\tau}} \tag{1}$$

where T_R is the receiver noise temperature, T_A is the antenna temperature, which typically ranges from 100 to 300 K, and B is the channel bandwidth, which typically ranges from 100 MHz for an O_2 channel to 1000 MHz for a window channel. Double-sideband noise temperatures T_R for room-temperature receivers range from approximately 500 K to 1500 K for frequencies ranging from 50 to 200 GHz, respectively. By cooling the receivers to 80 K, the receiver temperatures might vary from 400 K to 1000 K, respectively. Table 7 shows how the sensitivity of a typical 100-MHz O_2 channel with B =100 MHz and T_R =1000 K would depend on the scan parameters for a mapping time of 30 minutes. From Eq. 1, reductions in T_R below 100 to 200 K will not improve the sensitivity significantly.

The sensitivity of a filled-aperture sensor can be improved by employing several feed assemblies, each with a separate receiver, in a multiple-spot arrangement. By orienting a row of adjacent spots transverse to the scan direction, the desired area to be imaged is covered by wide swaths. In this case, the available integration time per spot is multiplied by the number of feed-plus-receiver assemblies N_f, hence the sensitivity is improved by $1/\sqrt{N_f}$. Due to the decreasing marginal cost of adding additional feed and receiver assemblies, the total cost of the feeds and receivers for the multiple-spot sensor should increase as $(N_f)^\alpha$, where $\alpha < 1$.

Perhaps a more significant advantage of a multiple-feed system for a mechanically scanned sensor is the reduction in the slew rate necessary for the physical scan of the primary beam-forming element. Consider a filled-aperture sensor using a parabolic reflector. For this case, satisfactory momentum compensation can be difficult to achieve for the maximum slew rates required by a single-spot sensor (Table 8). These rates are reduced by $1/N_f$ for the multiple-spot sensor. A reduction in slew rate of the parabolic reflector can also be achieved with a Cassegrain configuration employing a nutating subreflector. The light-weight subreflector scans the main beam at a high rate in a direction transverse to the slow raster motion of the main reflector. The required number of lateral spots for a 10°/min slew rate and 30-min mapping time are tabulated in Table 9 for various scan parameters. For either the multiple-feed or nutating-subreflector sensors, a main reflector with a large f/D ratio is desirable in order to minimize off-axis aberations at the extreme transverse spots.

Table 5: Required antenna beamwidth θ_{3dB} and diameter D for various spatial resolutions and channel frequencies.

Parameter		Equatorial Resolution R (km) 5	10	20	40	60
Beamwidth θ_{3dB} (arc min)		0.48	0.96	1.92	3.83	5.76
Aperture diameter D (m)	at 6 GHz	463	232	116	58	39
	at 18 GHz	154	77	39	19	13
	at 60 GHz	46	23	12	5.8	3.9
	at 118 GHz	23	12	5.9	2.9	2.0
	at 183 GHz	15	7.6	3.8	1.9	1.3
	at 220 GHz	13	6.3	3.2	1.6	1.0

Table 6: Available integration time (seconds) per spot for 30-min mapping of various sized regions for a single-spot sensor.

Area Diameter (km)	Equatorial Resolution R (km) 5	10	20	40	60
10,000 (full disk)	0.00045	0.0018	0.0072	0.029	0.065
4,000	0.0028	0.011	0.045	0.18	0.40
2,000	0.011	0.045	0.18	0.72	1.6

Table 7: Receiver sensitivity ΔT_{RMS} for 30-min mapping of various sized regions, assuming $T_R = 1000$ K and $B = 100$ Mhz.

Area Diameter (km)	Equatorial Resolution R (km) 5	10	20	40	60
10,000 (full disk)	4.8	2.4	1.2	0.59	0.39
4,000	1.9	0.95	0.47	0.24	0.16
2,000	0.95	0.47	0.24	0.12	0.08

Table 8: Required antenna scanning rates (°/min) for 30-minute mapping time of various sized regions.

	Equatorial Resolution R (km)				
Area Diameter (km)	5	10	20	40	60
10,000 (full disk)	900	450	225	112	75
4,000	144	72	36	18	12
2,000	36	18	9	4.5	3

Table 9: Required number of transverse spots for 10° /min scanning rate and 30-minute mapping time of various sized regions.

Area Diameter (km)	Equatorial Resolution R (km)				
	5	10	20	40	60
10,000 (full disk)	100	50	25	12	8
4,000	16	8	4	2	2
2,000	8	4	2	1	1

To minimize the angular and linear momentum transferred to the platform by any mechanically scanned elements, coaxial counter-rotating flywheels and collocation of the scanned element's pivot point with element's center of mass should be employed, as illustrated in Fig. 3. Active adjustment of this mechanism can be achieved by correcting the location of small masses attached to the antenna. This can be done using motorized actuators that respond to forces exerted by the antenna on the platform, as measured by strain gauges or other means.

Scattering from reflector surface irregularities reduces the main lobe efficiency by approximately $\exp[-(4\pi\epsilon/\lambda)^2]$, where ϵ is the RMS surface deviation from a true parabola. In order to achieve the desired main lobe efficiency levels, a filled-aperture reflector antenna will be required to have $\epsilon < \lambda/60$ for 95% main lobe efficiency, and $\epsilon < \lambda/75$ for 97% efficiency. At 220 GHz, these RMS deviation limits are 23μ (0.0009 in.) and 18μ (0.0007 in.), respectively. Scattering from struts and feed structures will further reduce the main lobe efficiency.

Diurnal exposure of the main beam-forming element to the sun's direct rays may necessitate some form of thermal stabilization. Aperture phase compensation for thermally induced distortions in a semi-rigid parabolic reflector surface can be achieved by using a series of motorized actuators placed between a supporting ring and the "petals" of the reflector (Fig. 4a-c), as defined by radial slits in the dish. The slits can be made narrow enough so that negligible main-lobe degradation occurs, and can be covered with a flexible foil to minimize edge diffraction. Alternate phase compensation concepts that would achieve equivalent results include Cassegrainian antenna configurations with controlled subreflector surfaces and phase-controlled sub-aperture feed assemblies.

The required amount of compensation can be determined by measuring the distance from the rear of the reflector to a suitable reference plane. Either capacitive or optical metrology could be used for the measurement, although any capacitive sensors should be shielded from the solar wind and light. The reference plane could be constructed from a tensioned membrane, which could be connected to the support ring at three points, or from a lightweight Invar bridgework.

Two-point calibration of a single- or multiple-feed sensor can be achieved by periodically moving a reflecting surface and then an absorbing load in front of the feed assembly. The reflector would be oriented to provide an unobstructed view of cold space, preferably within the ortho-ecliptic region. The absorbing load should be at a stable (± 1 K) temperature between 250 K and 350 K, and should be accurately monitored. Inefficiency in the main reflector would not be included in the calibration load measurements, but could be accounted for by measuring the reflector temperature and using *a-priori* knowledge of the reflector loss.

Other concepts for the implementation of large filled-aperture sensors include controlled-surface mesh, membrane, or segmented deployable antennas, Fresnel lenses, and phased-array bootlace lenses. In contrast to filled-aperture reflector antennas, filled-aperture lens antennas are relatively insensitive to small deviations in the lens profile, although lens concepts present other problems in meeting performance specifications over the wide range of frequencies required. In addition, due to minute variations in the insertion losses of the beam-forming elements as the array is scanned, the phased array may require a separate calibration at each spot. This might be performed using beacons positioned at many locations on the Earth.

4 Implementation using Synthetic-Aperture Sensors

Although synthetic aperture interferometers have been used successfully in radio astronomy for imaging point sources, their proposed application to the space-based imaging of extended objects such as the Earth is relatively new [13]. The spatial resolution of the synthesized aperture is related to the maximum element-pair separation distance by nearly the same relation as that of a filled aperture. Brightness sensitivities comparable to filled-aperture single-spot sensors can be obtained if all element-pair correlations are performed simultaneously.

An important issue which deserves attention is the possibility of excessively large near-, limb-, and ecliptic-sidelobes due to undersampling of the visibility function in the $u - v$ plane. This is of particular importance for thinned arrays. One part of the solution is to decrease the individual element field of view to the minimum allowable ($\sim 17.4°$), although this will increase the size of each element. Another part of the solution is to space the elements shoulder-to-shoulder, and then to have additional elements spaced at intermediate positions. Achievement of more than 95% beam efficiency in the synthesized pixels presents a significant challenge.

A practical system for the calibration of synthetic aperture sensors also needs to be developed. As in the case of the phased array, a calibration scheme employing Earth-located beacons might be used.

5 Summary

It is suggested that the science requirements for passive geostationary microwave observations be met by near- and far-term sensors for each of two overlapping bands (Fig. 5), with each band covering no more than a decade in frequency. The

low-frequency band includes channels near 6, 10, 18, 22, 31 to 37, and possibly 50 to 60 GHz. The high-frequency band includes channels near 220 to 230, 183, 166, 118, 90 to 110, and possibly 50 to 60 and 31 to 37 GHz. The precise channel specifications will have to comply with international frequency allocations [14].

The near-term goal is a high-frequency sensor based on a filled-aperture solid reflector antenna, which should rely on currently existing technology. The diameter of the reflector should be limited to 4.4 m (the size of the shuttle payload bay), which allows for a sensor partially exceeding the "adequate" spatial resolution requirements. Larger, deployable reflectors are not suggested for the near term unless the technology can be immediately demonstrated. The most critical issues for the near-term sensor are momentum compensation and the design of the feed assembly; these issues are coupled through the desired scan rate. Due to the nascent state of current large space antenna technology, no near-term goals for a low-frequency geostationary sensor are recommended.

The successful demonstration of the near-term (high-frequency) sensor will be essential for the continued development of far-term sensors satisfying the ideal science requirements. The far-term goal includes both a high-frequency sensor which meets the ideal science requirements, and a low-frequency sensor whose design will depend on advances in large antenna technology. The high-frequency sensor should consist of a filled-aperture controlled segmented or controlled semi-rigid antenna with a diameter from 10 to 40 meters.

The low-frequency (far-term) sensor might be based on one of several concepts : 1) a deployable mesh reflector antenna of diameter at least 20 m, which shows promise for use at frequencies up to 30-GHz, 2) a synthetic aperture interferometer of maximum baseline from 100 to 300 m, or 3) a deployable phased-array bootlace lens, of diameter from 100 to 300 m. The first of these, a deployable mesh reflector antenna, will satisfy only the adequate spatial resolution requirements. The last two concepts meet the ideal spatial resolution science requirements, although they present significant structural and meteorological challenges.

References

[1] J.W. Waters, K.F. Kunzi, R.L. Pettyjohn, R.K.L. Poon and D.H. Staelin, "Remote Sensing of Atmospheric Temperature Profiles with the Nimbus-5 Microwave Spectrometer", *J. Atm. Sci.*, Vol. 32, No. 10, 1975.

[2] A.D.S. Ali, P.W. Rosenkranz and D.H. Staelin, "Atmospheric Sounding Near 118 GHz", *J. Appl. Meteorol.*, Vol. 19, No. 10, 1980.

[3] D.H. Staelin, K.F. Kunzi, R.L Pettyjohn, R.K.L. Poon, P.W. Rosenkranz and

J.W. Waters, "Remote Sensing of Atmospheric Water Vapor and Liquid Water with the Nimbus-5 Microwave Spectrometer", *J. Appl. Meteorol.*, Vol. 15, No. 11, 1976.

[4] P.W. Rosenkranz, M.J. Komichak and D.H. Staelin, "A Method for Estimation of Atmospheric Water Vapor Profiles by Microwave Radiometry", *J. Appl. Meteorol.*, Vol. 21, No. 9, 1982.

[5] T.T. Wilheit, A.T.C. Chang, M.S.V. Rao, E.B. Rodgers and J.S. Theon, "A Satellite Technique for Quantitatively Mapping Rainfall Rates over the Oceans", *J. Appl. Meteorol.*, Vol. 16, No. 5, 1977.

[6] R.W. Spencer, "A Satellite Passive 37-GHz Scattering-based Method for Measuring Oceanic Rain Rates", *J. Climate. Appl. Meteor.*, Vol. 25, No. 6, 1986.

[7] ———, J.W. Barrett, P.G. Bonanni and D.H. Staelin, "Aircraft-Based Radiometric Imaging of Tropospheric Temperature Profiles and Precipitation Using the 118.75-GHz Oxygen Resonance", Accepted for publication in *J. Appl. Meteorol.*, 1988.

[8] G.M. Heymsfield and R. Fulton, "Comparison of High-Altitude Remote Aircraft Measurements with the Radar Structure of an Oklahoma Thunderstorm: Implications for Precipitation Estimation from Space", *Mo. Wea. Rev.*, Vol. 116, No. 5, 1988.

[9] I.M. Hakkarinen and R.F. Adler, "Observations of Precipitating Convective Systems at 92 and 183 GHz: Aircraft Results", *Meteorol. Atmos. Phys.*, Vol. 38, 1988.

[10] H.F. Hawkins and S.M. Imbembo, "The Structure of a Small, Intense Hurricane-Inez 1966", *Mo. Wea. Rev.*, Vol. 104, 1966.

[11] R.W. Spencer, H.M. Goodman and R.E. Hood, "Precipitation Retrieval Over Land and Ocean with the SSM/I, Part 1: Identification and Characteristics of the Scattering Signal", Accepted for publication in *J. Atmos. Ocean. Technology*, 1988.

[12] S. Silver, *Microwave Antenna Theory and Design*, McGraw-Hill, New York, 1949.

[13] C.S. Ruf, C.T. Swift, A.B. Tanner and D.M. Le Vine, "Interferometric Synthetic Aperture Microwave Radiometry for the Remote Sensing of the Earth", *IEEE Trans. Geosci. Remote Sensing*, Vol. 26, No. 5, 1988.

[14] Litman, V. and J. Nicholas, *Guidelines for Spaceborne Microwave Sensors*, NASA Reference Publication 1086, National Technical Information Service, Springfield, Virginia, March, 1982.

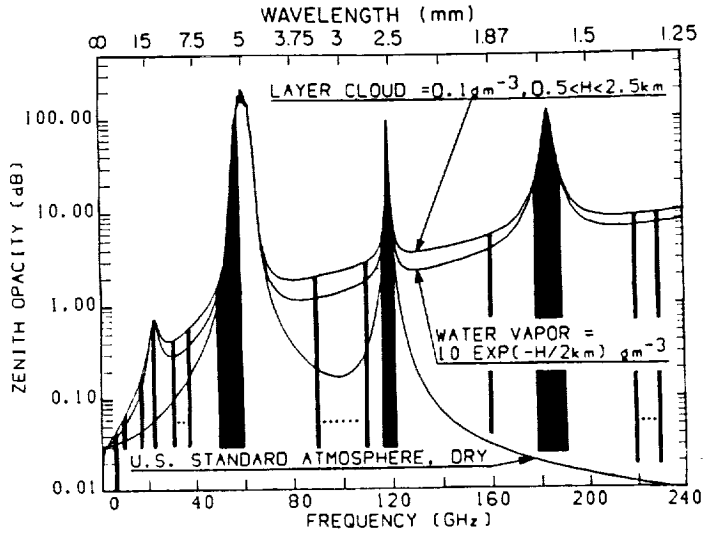

Figure 1: Zenith microwave opacity spectrum of the atmosphere for dry, moist, and cloudy conditions. Channels useful for the sounding of tropospheric temperature, water vapor, clouds, and precipitation are indicated by dark bars; the dots indicate regions over which only a single channel is needed.

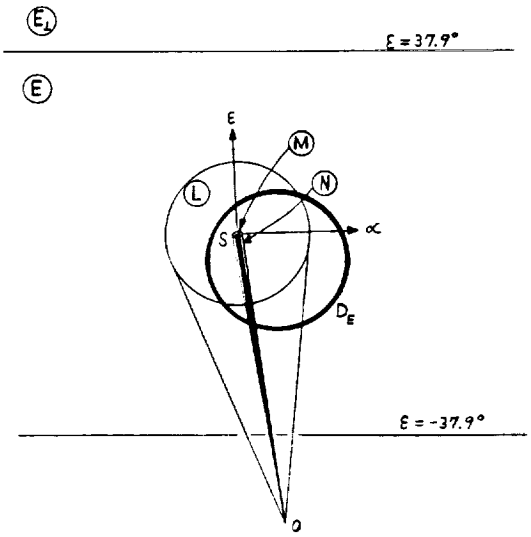

Figure 2: Angular regions for the specification of sidelobe levels and main lobe efficiency for a geosynchronous passive microwave sensor. O is the sensor position, D_E is the outline of the Earth's disk, S is the observed spot, M is the main lobe region, N is the near-sidelobe region, L is the limb-sidelobe region, E is the ecliptic-sidelobe region, $E_\perp$ is the ortho-ecliptic sidelobe region, and ϵ and α define elevation and azimuthal directions relative to the antenna boresight.

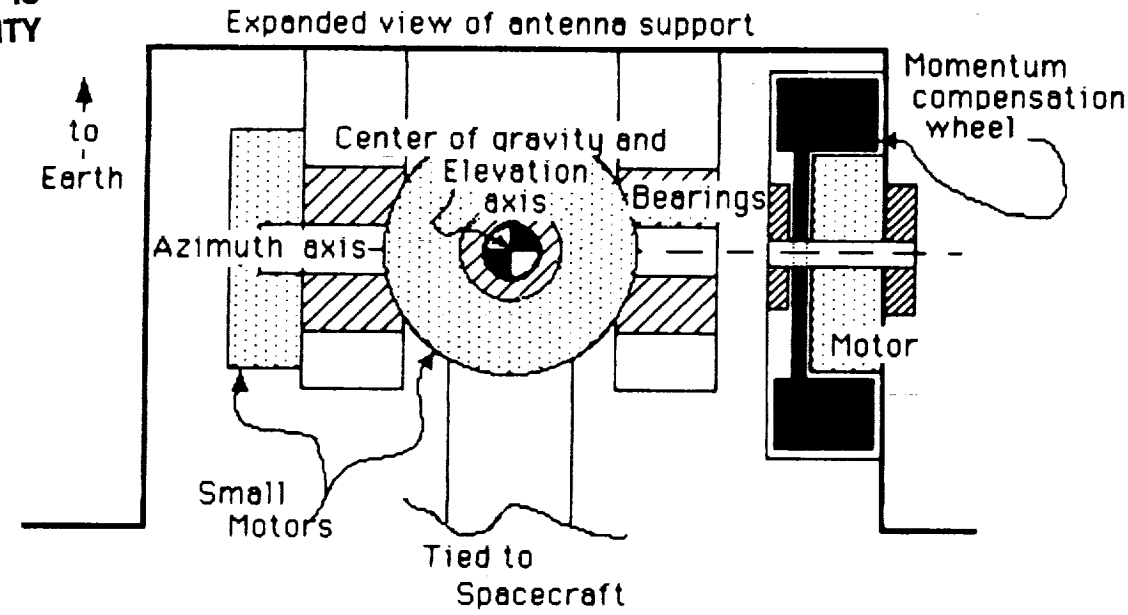

Figure 3: Schematic view of a coaxial angular momentum compensation technique. The antenna pivot is located at the center of mass to minimize the linear momentum transferred to the platform. The momentum wheel axes also pass through the center of mass to minimize excitation of platform vibration modes.

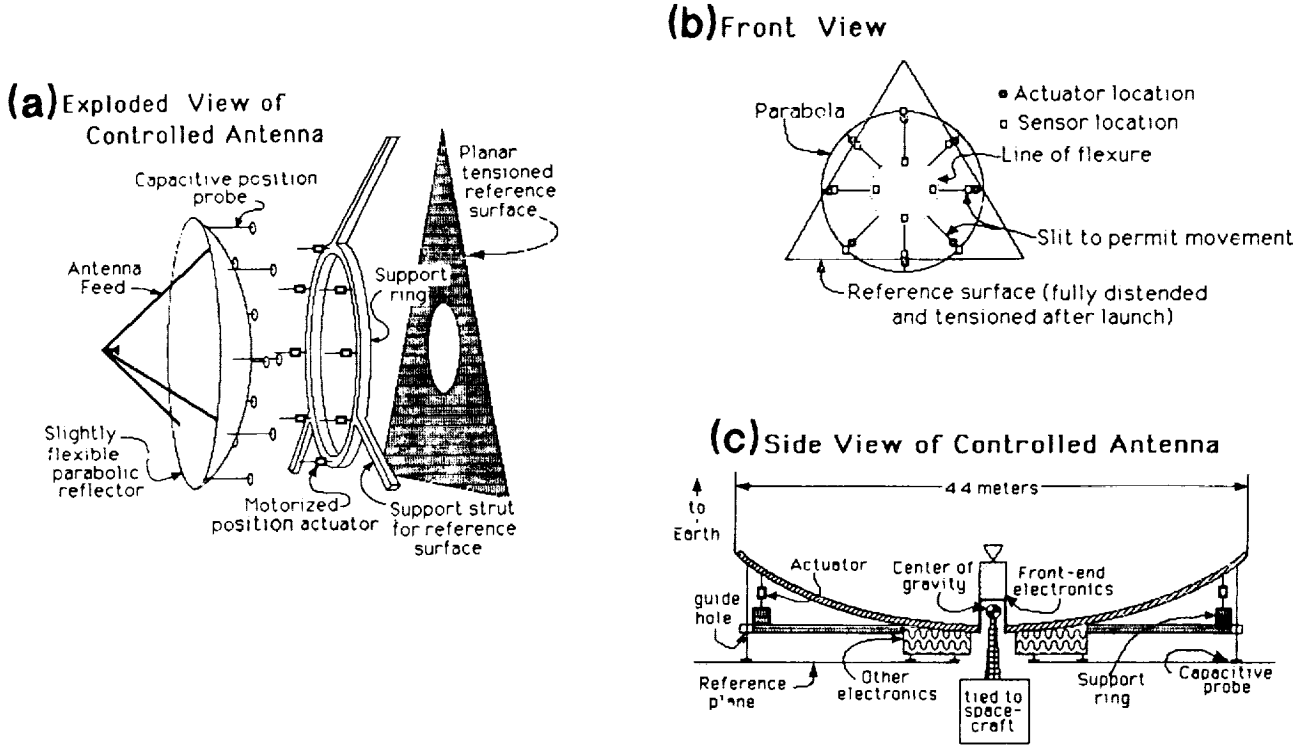

Figure 4: Schematic view of a mechanically scanned sensor employing a controlled, semi-rigid parabolic reflector antenna. (a) Exploded view illustrating reflector, support ring and planar reference surface. (b) Front view illustrating the reflector petals formed by radial slits. (c) Side view illustrating the reflector pivot location and capacitive metrology system.

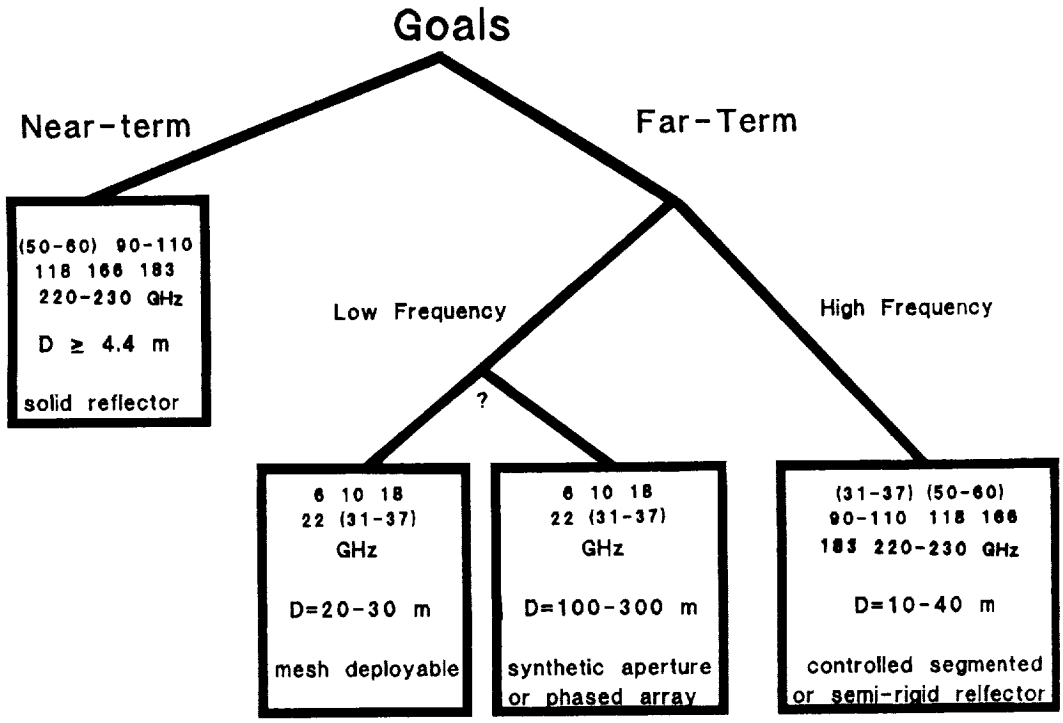

Figure 5: Suggested near- and far-term sensors for geosynchronous passive microwave observation.